Evaluation of numerical methods for explicit chemistry integration and application on DNS of turbulent kerosene ignition at high altitude conditions

A. Pestre*[,1], B. Cuenot[1], E. Riber[1]

[1]CERFACS, 42 avenue Gaspard Coriolis, TOULOUSE 31057, France

Abstract

Ignition at high altitude realistic conditions is a critical aspect of aeronautical engine certification and requires an accurate chemical description. For this study, two-dimensional ignition simulations triggered by energy deposition are performed to evaluate numerical strategies for chemistry integration. First, Analytically Reduced Chemistry with the Quasi-Steady-State Approximation is developed and used. The comparison with the reference skeletal scheme presents some differences on the transition from auto-ignition to flame propagation but a reasonable agreement is observed for the overall ignition sequence and the CPU cost is largely reduced. Then, an exponential integration of chemistry and an automatic sub-cycling procedure are presented. These methods enable further CPU-cost reduction while keeping a correct precision on the results. Finally, the combination of these methods is applied to a three-dimensional DNS of turbulent kerosene ignition.

Introduction

High altitude relight is a critical aspect of the design and certification of aeronautical engines. The low pressure and low temperature conditions have shown strong influences on the complex phenomena involved in ignition [1]. In order to evaluate the effect of these conditions on the chemical structure of the flame kernel, detailed kinetic schemes are required. However, such schemes cannot be used directly in DNS computations because of their excessively high numerical cost due to too many species to transport and a high stiffness requiring very low time steps. To overcome these issues, several numerical methods for the chemistry integration are proposed and evaluated in terms of precision and CPU (Central Processing Unit) cost. A reduced chemistry for kerosene-air ignition applications is first developed. Then the exponential integration of the chemistry is detailed with the sub-cycling procedure. Finally, the application of these methods is presented on 2D laminar configurations and then tested on a 3D turbulent ignition DNS computation.

Numerical set up

To evaluate several chemistry integration methods in the context of kernel ignition, a two-dimensional square configuration is first chosen. The domain size $1cm \times 1cm$ and 401 points are used in each direction to discretize the domain ($\Delta x = 25\,\mu m$). The resulting discretization allows to have around 40 points in the thermal flame thickness which ensures the spatial resolution required for combustion processes with a detailed chemical mechanism. The domain is initially filled with a gaseous premixed mixture of kerosene-air at stoichiometry, at low temperature ($T = 233\,K$), and at low pressure ($P = 0.3\,bar$).

The ignition and the kernel formation are triggered by an energy deposition in the center of the domain. The temperature increase causes chemical runaway with auto-ignition processes, which then form a hot kernel with a spherical propagative flame front. The energy deposition model is similar to the one used in [2]. Hence, the energy source term applied to the energy conservation equation follows a Gaussian shape both in time and space:

$$E_s(x,y,z,t) = \frac{\epsilon_i}{\sqrt{2\pi}^{n+1}\sigma_t\sigma_s^n} e^{\frac{(t-t_0)^2}{2\sigma_t^2}} e^{\frac{(x-x_0)^2+(y-y_0)^2+(z-z_0)^2}{2\sigma_s^2}} \quad (1)$$

where ϵ_i is the amount of energy deposited. x_0, y_0, z_0, are the coordinates of the deposit center, and t_0 is the time corresponding to the maximum energy deposition. n is the dimension of the computation.σ_s and σ_t are the characteristic size and duration of the deposit respectively, and are derived from the Gaussian standard deviation such as the amplitude at a distance $\Delta_{s,t}$ is one thousandth of the amplitude at the deposition center:

$$\Delta_{s,t} = \sigma_{s,t} \times \sqrt{2\ln(10^4)} \quad (2)$$

For this study the deposition duration is $2\Delta_t = 100\,\mu s$, and the radius is $\Delta_s = 5\,mm$. However due to the Gaussian shape, the main part of the energy (70%) is deposited in a spherical volume of $2\,mm$ radius and during the time interval $[30\,\mu s\,;\,70\,\mu s\,]$. The energy deposited $\epsilon_i = 16.65\,mJ.cm^{-1}$ is chosen to reach a maximum temperature of $3000K$ without chemical reactions.

The DNS structured code NTMIX [3] is used for this study. It resolves reacting Navier-Stokes flow equations with a centered explicit finite difference scheme of order 6 and a temporal Runge-kutta scheme. Complex transport properties are considered with the computation of individual species to mixture diffusion coefficients from binary coefficients. The Navier-Stokes Characteristic Boundary Conditions (NSCBC)

* Corresponding author: pestre@cerfacs.fr

formalism [4] is used to avoid reflecting pressure waves at the boundary conditions due to the deposited energy.

Chemistry reduction

In this work the hierarchical kinetic mechanism developed by the CRECK Modeling group [5] has been chosen as reference. It is composed of 491 species and 15276 reactions allowing an accurate description of C1 to C16 carbonated species with high and low temperature chemistries. The fuel chosen for this study is a multi-component surrogate composed of three species that emulate the behavior of the Jet-A1 used in aeronautical engines. The composition by molar fraction is n-dodecane (60%) representing the paraffin behavior, methylcyclohexane (20%) that stands for the cyclic species, and o-xylene (20%) for the aromatics [6].

For 3D and 2D flow simulations, it is mandatory to reduce the number of species, reactions, and the stiffness of the chemistry [7]. Hence, a first skeletal scheme is derived with the software ARCANE [8] using DRGEP method [9] and a linear lumping [10]. The reactions rate coefficients are not changed and all the unnecessary species and reactions are discarded. This skeletal scheme obtained is composed of 52 transported species and 310 reactions. It will be named S52R310 in the following, and will be considered as reference. Then, the ARC (Analytically Reduced Chemistry) is obtained by applying the Quasy-Steady-State Approximation (QSS) [11]. Under this assumption, species with a very short characteristic timescale are considered to have zero net chemical source term and can be computed through algebraic expression from the other species. Therefore, they are not resolved by the CFD solver, which reduces the chemical stiffness and the CPU cost. The ARC scheme obtained here is composed of 30 transported species, 299 reactions, and 22 QSS species. It will be named S30R299QSS22 in the following. These reductions have been performed using 1D premixed flames at low pressure and low temperature conditions conserving accurately the laminar flame speed, the adiabatic temperature, and final species mass fractions of the main products (CO_2, CO, H_2O). Constant pressure auto-ignition reactors at low pressure and initial temperature $T_i = 1600K$ and $T_i = 3000K$ have also been used to target the ignition time. Figures 1 and 2 show the validation of these two schemes. An overall good agreement is observed on the laminar flame speed on the whole range of flammability with less than 5% error. For the auto-ignition time, good results are observed for temperature higher than $T_i = 1200K$, the lower temperatures being not targeted for ignition in this study. Indeed, it is observed for this set-up with energy deposition, that the chemical runaway occurs around $T = 1600K$. For high temperatures close to $T_i = 3000K$ the heat release peak used to define the auto-ignition spreads out, thus, the measurement of the auto-ignition time becomes less trustworthy.

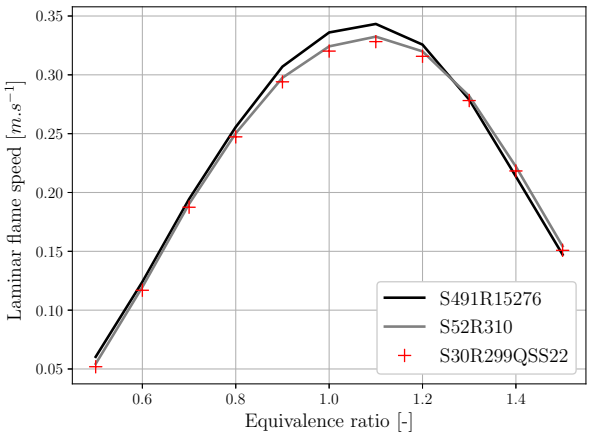

Figure 1: Laminar flame speed versus equivalence ratio in a 1-dimensional premixed flame at $P = 0.3\ bar$ and $T = 233\ K$: comparison of reduced schemes with the reference detailed scheme.

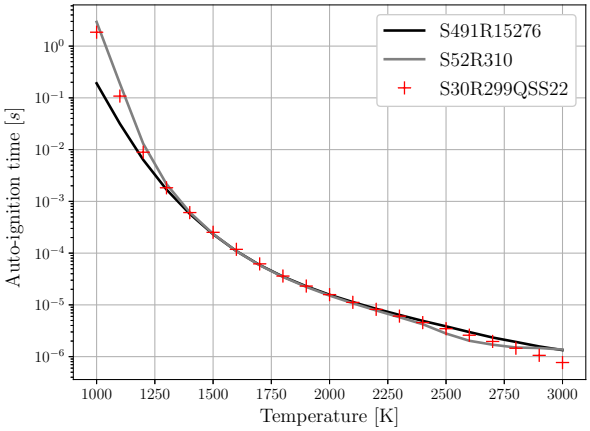

Figure 2: Auto-ignition time versus initial temperature in a 0-dimensional constant pressure reactor with stoichiometric mixture at $P = 0.3\ bar$: comparison of reduced schemes with the reference detailed scheme.

Chemistry integration

In the classical chemistry integration, the species production rates $\omega_k^{\cdot}$ are computed from the reaction rates of progress $\mathcal{Q}_j$ [12]:

$$\omega_k^{\cdot} = \sum_{j=1}^{N_{react}} \omega_{k,j}^{\cdot} = W_k \sum_{j=1}^{N_{react}} \nu_{k,j}\, \mathcal{Q}_j \qquad (3)$$

where W_k is the molar mass of species k, and $\nu_{k,j} = \nu''_{k,j} - \nu'_{k,j}$ is the net stoichiometric coefficient in reaction j.

$$\mathcal{Q}_j = K_{fj} \prod_{k=1}^{N_{spec}} [X_k]^{\nu'_{k,j}} - K_{rj} \prod_{k=1}^{N_{spec}} [X_k]^{\nu''_{k,j}} \qquad (4)$$

where $[X_k]$ is the molar concentration of species k. K_{fj} and K_{rj} are the forward and backward reaction rates respectively and are computed from Arrhenius laws and thermodynamic equilibriums. Integrating very fast

chemistry with explicit time schemes leads to very small time steps. Implicit integration allows larger time steps but at the cost of accuracy and complexity. In addition, it requires to solve an inverse problem which may turn very costly.

A simpler approach is proposed here, based on the analytical form of the integration of the chemical source term. Assuming that species are produced and consumed following a first order differential equation, the chemical problem may be written as [13]:

$$\frac{dc_k}{dt} = \dot{\omega}_k = A_k c_k + B_k \quad (5)$$

where $A_k c_k$ and B_k are the contribution to destruction and creation respectively:

$$A_k c_k = \sum_{j=1}^{N_{react}} \omega_{k,J}^{\cdot} \text{ for all } \omega_{k,J}^{\cdot} < 0 \quad (6)$$

$$B_k = \sum_{j=1}^{N_{react}} \omega_{k,J}^{\cdot} \text{ for all } \omega_{k,J}^{\cdot} > 0 \quad (7)$$

The solution of Eq. (5) has the form:

$$c_k(t) = \left(c_{k,0} + \frac{B_k}{A_k}\right) e^{A_k t} - \frac{B_k}{A_k} \quad (8)$$

where $c_{k,0} = c_k(t = 0)$. Eq. (8) can be discretized into:

$$c_k^{n+1} = \left(c_k^n + \frac{B_k^n}{A_k^n}\right) e^{A_k^n \Delta t} - \frac{B_k^n}{A_k^n} \quad (9)$$

This expression has the property to be always positive and the exponential term enables a smooth exponential damping for large time steps. Hence, the exponential formalism is more numerically stable. However, the counterpart is the non-atom conservation which increases with large time steps. To avoid this issue, a mass conservation algorithm is applied after the exponential integration [13].

In addition to this method a dynamical and local sub-cycling procedure is also applied. At each iteration, a number of chemical sub-cycles is determined to divide the time step of the current iteration (Δt) into smaller time steps ($\Delta t_{chem-SC} = \Delta t / N_{Sub-Cyc}$) used only for the chemistry integration. This allows a better precision and stability for the computation of the chemical production terms without re-evaluating all the Navier-Stokes Right Hand Side (RHS) terms. The number of sub-cycles is based on conditions of Eq. (10) and (11), where $\Delta t_{chem,k}$ is the time interval corresponding to 1% variation of the concentration of species k.

$$\Delta t_{chem,k} = \frac{c_k}{\dot{\omega}_k} \times 0.01 \quad (10)$$

$$N_{Sub-Cyc} = \min\left[\max\left(\frac{\Delta t}{\Delta t_{chem,k}}, 1\right), M_{SC}\right] \quad (11)$$

M_{SC} is a user parameter defining the maximum number of sub-cycles in the computation. Indeed, the condition Eq. (10) provides very low chemical time steps, and so, a large number of sub-cycles that may not necessary and too costly. The user parameter allows to control the balance precision/cost. This procedure can be seen as a chemical sensor with Eq. (10) that indicates where sub-cycles are needed.

Test cases

To evaluate the performances of the methods presented in the previous section, several simulations have been performed. Table 1 summarizes these simulations with the corresponding labels and methods used.

Label	Scheme	Method	M_{SC}	Δt factor
KD1000	Skeletal	Classic	1	0.001
CD50	ARC	Classic	1	0.02
CD10	ARC	Classic	1	0.1
C	ARC	Classic	1	1
CS10	ARC	Classic	10	1
ED10	ARC	Expo	1	0.1
E	ARC	Expo	1	1
ES10	ARC	Expo	10	1

Table 1: Summary of simulations and methods used

All the simulations are based on CFL and Fourier conditions for the computation of the time step. This time step reaches the minimum value of $\Delta t = 9.1\ ns$ during the kernel formation. However, due to the stiffness of the chemistry, the computation of the production terms can require lower time steps. In this case, the CFL and Fourier numbers are reduced. This reduction corresponds to the Δt factor in Tab. 1. For example, the case KD1000 uses a time step divided by 1000 ($\Delta t = 9.1 \times 10^{-12} s$) compared to the one based on convective and diffusive stability limits only.

Evaluation of the QSS formalism

First, the influence of the chemical scheme and the QSS species is evaluated for ignition. The ARC formalism becomes more and more attractive for reactive CFD applications [14], and it has been used in several configurations [15-16]. However, few studies have provided a direct comparison between skeletal and ARC scheme in ignition cases with thermal chemical runaway. The physics of these phenomenon are hard to simulate as it implies many radical species in a transitory regime with very short time scales.

The comparison between the cases KD1000 and CD50 on Fig. 3 shows large differences on the heat release rate profiles at the first instants. The skeletal scheme leads to larger heat release resulting in a faster temperature increase on Fig. 4. The temporal evolution indicates that the auto-ignition happens at the same time for both chemistries, but differs in the transition phase

leading to propagative front. Fig. 3. shows that this transition occurs faster with the skeletal scheme. Indeed, at $t = 60\mu s$ the flame front starts to form, and the heat release rate starts to decrease in the kernel center. On the contrary, for the ARC scheme the kernel center remains the most active zone. This difference in the transition phase creates a delay between the two simulations. Hence, at later times, the flame front of case KD1000 precedes the one of case CD50. There is also a slight difference on the maximum value of the heat release rate during the flame propagation, however it is compensated by the larger flame front in the ARC computation which leads then to the same flame speed.

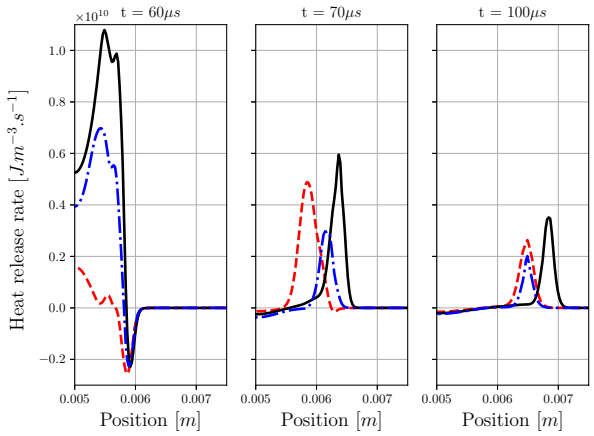

Figure 3: Heat release rate radial profiles at several instants. Black curve: case KD1000 ; red dashed curve: case CD50 ; blue dash-dotted line : scheme S31R310QSS21.

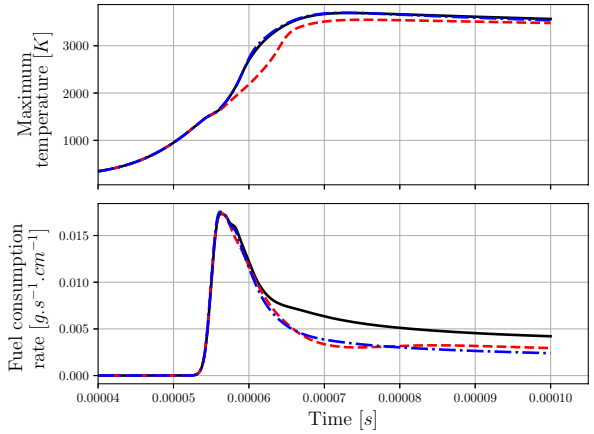

Figure 4: Temporal evolutions of maximum temperature (top) and fuel consumption rate (bottom). Black curve: case KD1000 ; red dashed curve: case CD50 ; blue dash-dotted line : scheme S31R310QSS21.

The time steps used in cases KD1000 and CD50 are different but a simulation of CD50 with a time step divided by one thousand leading to the same results demonstrates that the differences can only be explained by the QSS species.

Indeed, Fig. 5 shows the higher total production rate in case KD1000 for species that have been put in QSS assumption. These species do not respect this assumption since their production rate is not equal to 0, especially for CH_2CO. The chemical scheme S31R310QSS21 corresponds to the ARC scheme with CH_2CO which is transported. Blue curve on Fig. 3 and 4 indicates an improved precision with this new scheme. Better results could be obtained by transporting the other species presented in Fig. 5. However, the stiffness of this new scheme is too high, and it has been chosen to keep the scheme S30R299QSS22 in the following.

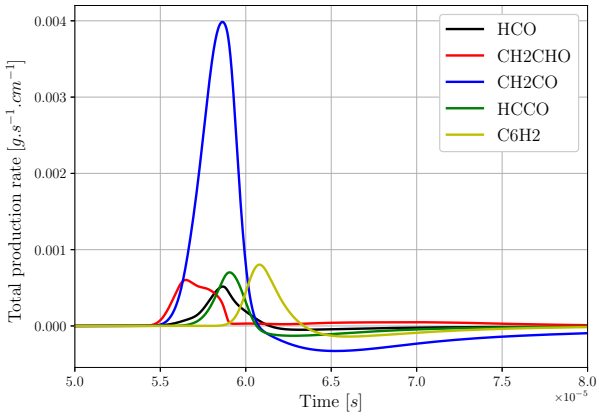

Figure 5: Evolution of total production rate in case KD1000 for species set in QSS in case CD50.

Despite the differences observed on Fig. 3, the temporal evolutions on Fig. 4 indicate similar behaviors once the flame kernel is formed ($t > 80\mu s$). The maximum temperature shows only $50K$ difference, and the fuel consumption rates have the same evolution (the offset is due to the larger kernel radius in the KD1000 case). The computations using ARC are far richer in terms of physical information and precision than single or two step chemistries often used in DNS studies [17].

Computational gains from a case A to a case B are expressed using the following factors:

$$R^{\Delta t}_{A\to B} = \frac{\Delta t_B}{\Delta t_A} \quad \text{and} \quad K^{cpu}_{A\to B} = \frac{t^{cpu}_B}{t^{cpu}_A} \tag{12}$$

$R^{\Delta t}_{A\to B}$ represents the reduction of the stiffness while $K^{cpu}_{A\to B}$ takes also into account the reduction of species transported and the cost of the chemistry integration. The computational gains from skeletal to ARC chemistry are presented in Tab. 2 and show a large reduction of the stiffness and CPU cost. Hence, the ARC chemistry offers a good cost/precision compromise. Note that, at this stage, the ARC scheme is still too stiff for a 3D simulation, and the time-step is limited by chemistry.

Case A	Case B	$R^{\Delta t}_{A\to B}$	$K^{cpu}_{A\to B}$
KD1000	CD50	20	0.025
CD50	ED10	5	0.223
ED10	ES10	10	0.233
KD1000	ES10	1000	0.0013

Table 2: Summary of computational gains

Exponential chemistry integration

The comparison between exponential and explicit chemistry integration is presented on Fig. 6. The results are identical for the cases CD50 and ED10. Thus, the exponential integration allows to use larger time steps without compromising the precision.

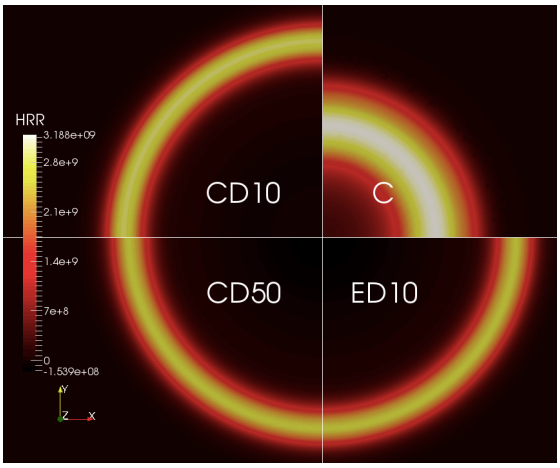

Figure 6: Comparison of the heat release rate field at the end of the energy deposition for cases C, CD10, CD50, and ED10.

The gains are presented in Tab. 2 (second line) demonstrating the interest of this integration method.

The cases CD50, CD10, and C, show the effect of the temporal discretization on explicit chemistry integration. While the C case clearly provides a wrong solution, the computation with the time step divided by 10 shows a reasonably good agreement with only a small shift of the flame front and a slightly higher heat release rate at the center. In this case, the exponential integration does not improve the CPU performances.

A comparison has been also done between cases E, C (no time step reduction), and ED10. The case E predicts well the kernel structure while case C is far. However, case E exhibits stability issues at the center of the domain and at some points of the flame front. This result means that exponential chemistry integration allows to use larger time steps, but also has a discretization limit for stability.

Sub-cycling procedure

The effect of sub-cycling can be seen on Fig. 7. For the exponential integration, the sub-cycling procedure is exactly equivalent to the reduction of the time-step. Indeed, cases ED10 and ES10 have the same heat release rate field. For explicit integration this is not the case, on the contrary, it seems that the sub-cycles worsen the heat release rate prediction compared to the C case. This phenomenon could be explained by small oscillations of the production rates. Indeed, without sub-cycling, diffusion smoothes the solution at each iteration, whereas with sub-cycling, diffusion is computed each 10 chemical sub-cycles. Further studies are needed to validate this assumption. Meanwhile, these results indicate that the sub-cycling procedure is not adapted to explicit chemistry integration for ignition.

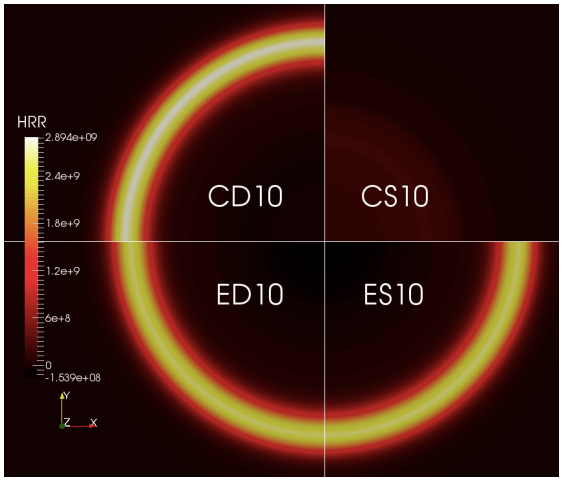

Figure 7: Comparison of the heat release rate field at the end of the energy deposition for cases CS10, CD10, ED10, and ES10.

The gain observed with the sub-cycling procedure for exponential integration is presented in Tab. 2 (third line). Even if with sub-cycling the chemistry is more expensive, it is compensated by the time step increase. This cost is even more reduced in 3D simulations since the computation of the third direction reduces the relative cost of chemistry.

At this stage, the time step is no more limited by chemistry, but by the CFL and Fourier conditions. Hence, the gain still could be increased on coarser meshes by adding more sub-cycles.

Application to the 3D turbulent ignition

Finally, the total gain factor obtained with the combination of all the presented methods is presented in the last line of Tab. 2. Hence, the time step has been multiplied by 1000 and the CPU cost divided by 769. It is now possible to consider a 3D DNS ignition simulation in a turbulent flow with a reasonably precise kerosene-air chemistry.

For the 3D computation the flow is initially a homogeneous and isotropic turbulence with the turbulent Reynolds number $Re_t = 917.2$. The turbulent integral scale used is $L_t = 4.17mm$. The domain length is $L = 2.5\ cm$ with 501 points per direction ($\Delta x = 50\ \mu m$) to ensure at least 6 turbulent structures per direction. The energy deposition has the same characteristics except for the amount of energy deposited which is adapted to 3D: $\epsilon_i = 3.18\ mJ$. The ARC scheme is used with the exponential chemistry integration and the maximum number of sub-cycles is set to $M_{SC} = 40$.

The resulting kernel formation and deformation by turbulent structures is displayed on Fig. 8. At the low pressure and low temperature conditions the reactivity is reduced. Thus, the turbulence has a strong influence on the kernel and pockets are detached from the main core. The computational cost is 53909 cpu-hours for 200µs simulated. The objective here is to demonstrate the feasibility of such computation and the interest of the presented methods. The physical analysis of the

kerosene-air ignition with the low pressure and low temperature effects will be evaluated in another dedicated study.

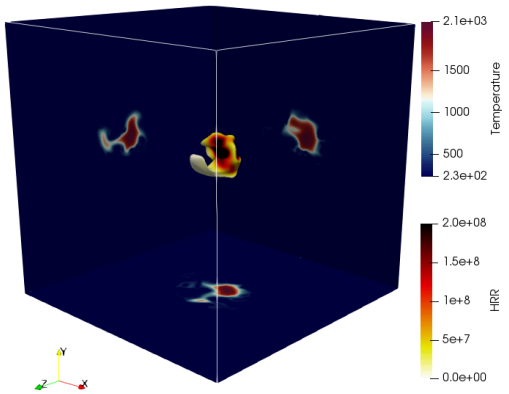

Figure 8: Visualization of the flame kernel at $t = 200\,\mu s$ with iso-contour $T = 1000K$ colored by heat release rate and projected temperature field.

Conclusion

Several approaches for chemistry integration have been evaluated in the context of kerosene-air ignition with energy deposition. First the ARC chemistry formalism has been compared with the skeletal scheme from which it is derived. Despite differences observed during the transition phase from auto-ignition to flame front propagation, the ARC scheme is able to reproduce the main ignition mechanisms and provides a similar evolution once the flame kernel is formed. The main advantage of the ARC chemistry is the reduced stiffness of the chemistry and the reduced number of species transported which finally allows to divide the CPU cost by 40 in this study. Then a new exponential integration method associated to a sub-cycling procedure has been presented. This methodology is more stable numerically, and enables to further increase the computational time step while keeping the same precision. At the end, the time step is only limited by CFL and Fourier conditions. All these methods result in a total CPU cost divided by 769. It is then possible to run a 3D DNS simulation of a turbulent kernel ignition with a reasonably precise kerosene-air chemistry.

Acknowledgements

This work was performed in the context of the APLAREP project funded by Safran Aircraft Engine, and using HPC resources from GENCI- TTGC (Grant 2020-A0052B10157).

References

[1] Martinos, A., Palanti, L., Harth, S., Andreini, A., Zarzalis, N., Trimis, D., & Vitale, I. (2019). Analysis of ignition processes at combustors for aero engines at high altitude conditions. *Proceedings of the European Combustion Meeting*.

[2] Lacaze, G., Richardson, E., & Poinsot, T. (2009). Large eddy simulation of spark ignition in a turbulent methane jet. *Combustion and Flame*.

[3] Baum, M., (1994). Etude de l'allumage et de la structure des flammes turbulentes. *PhD*.

[4] Baum, M., Poinsot, T., & Thévenin, D. (1995). Accurate boundary conditions for multicomponent reactive flows. *Journal of Computational Physics*.

[5] Ranzi, E., Frassoldati, A., Stagni, A., Pelucchi, M., Cuoci, A., & Faravelli, T. (2014). Reduced kinetic schemes of complex reaction systems: Fossil and biomass-derived transportation fuels. *International Journal of Chemical Kinetics*.

[6] Humer, S., Seiser, R., & Seshadri, K. (2011). Experimental investigation of combustion of jet fuels and surrogates in nonpremixed flows. *Journal of Propulsion and Power*.

[7] Lu, T., Law, C. K., Yoo, C. S., & Chen, J. H. (2009). Dynamic stiffness removal for direct numerical simulations. *Combustion and Flame*.

[8] Cazères, Q., Pepiot-Desjardins, P., Riber, E., Cuenot, B., A fully automatic procedure for the analytical reduction of chemical kinetics mechanisms for Computational Fluid Dynamics applications, *submitted to FUEL*.

[9] Pepiot-Desjardins, P., & Pitsch, H. (2008). An efficient error-propagation-based reduction method for large chemical kinetic mechanisms. *Combustion and Flame*.

[10] Pepiot-Desjardins, P., & Pitsch, H. (2008). An automatic chemical lumping method for the reduction of large chemical kinetic mechanisms. *Combustion Theory and Modelling*.

[11] Lu, T., & Law, C. K. (2006). Systematic approach to obtain analytic solutions of quasi steady state species in reduced mechanisms. *Journal of Physical Chemistry A*.

[12] Poinsot, T., & Veynante, D. (2012). *Theoretical and Numerical Combustion* (3nd ed.).

[13] Blanchard, S., Cuenot, B., Cazeres, Q., Chemical modelling for methane oxy-combustion in Liquid Rocket Engines, *submitted to Journal of Propulsion and Power*.

[14] Felden, A., Pepiot, P., Esclapez, L., Riber, E., & Cuenot, B. (2019). Including analytically reduced chemistry (ARC) in CFD applications. *Acta Astronautica*.

[15] Collin-Bastiani, F., Vermorel, O., Lacour, C., Lecordier, B., & Cuenot, B. (2019). DNS of spark ignition using Analytically Reduced Chemistry including plasma kinetics. *Proceedings of the Combustion Institute*.

[16] Felden, A., Riber, E., & Cuenot, B. (2018). Impact of direct integration of Analytically Reduced Chemistry in LES of a sooting swirled non-premixed combustor. *Combustion and Flame*.

[17] Turquand d'Auzay, C., Papapostolou, V., Ahmed, S. F., & Chakraborty, N. (2019). On the minimum ignition energy and its transition in the localised forced ignition of turbulent homogeneous mixtures. *Combustion and Flame*.